NEURO-ONCOLOGY

Matrix metalloproteinase-2 regulates vascular patterning and growth affecting tumor cell survival and invasion in GBM

Rose Du, Claudia Petritsch, Kan Lu, Patty Liu, Anna Haller, Ruth Ganss, Hanqiu Song, Scott Vandenberg, and Gabriele Bergers

Departments of Neurological Surgery (R.D., C.P., K.L., P.L., A.H., H.S., S.V., G.B.) and Pathology (S.V.) and Brain Tumor Research Center and Comprehensive Cancer Center (C.P., G.B.), University of California San Francisco, San Francisco, CA, USA; Department of Neurological Surgery, Brigham and Women's Hospital, Harvard Medical School, Boston, MA, USA (R.D.); Western Australian Institute for Medical Research, Perth, Australia (R.G.)

Glioblastoma multiforme (GBM) is one the most aggressive brain tumors due to the fast and invasive growth that is partly supported by the presence of extensive neovascularization. The matrix metalloproteinase MMP-2 has been associated with invasive and angiogenic properties in gliomas and is a marker of poor prognosis. Since MMP-2 is expressed in both tumor cells and endothelial cells in GBM, we generated genetically engineered MMP-2 knockout (MMP-2ko) GBM to examine the importance of the spatial expression of MMP-2 in tumor and/or normal host-derived cells. MMP-2–dependent effects appeared to be dose-dependent irrespective of its expression pattern. GBM completely devoid of MMP-2 exhibited markedly increased vascular density associated with vascular endothelial growth factor receptor 2 (VEGFR2) activation and enhanced vascular branching and sprouting. Surprisingly, despite the high vascular density, tumor cells were more prone to apoptosis, which led to prolonged survival of tumor-bearing mice, suggesting that the increased vascularity is not functional. Congruently, tumor vessels were poorly perfused, exhibited lower levels of VEGFR2, and did not undergo proper maturation because pericytes of MMP-2ko tumors were not activated and were less abundant. As a result of impaired and dysfunctional angiogenesis, MMP-2ko GBM became more invasive, predominantly by migrating along blood vessels into the brain parenchyma. *Neuro-Oncology 10, 254–264, 2008 (Posted to Neuro-Oncology [serial online], Doc. D07-00081, March 21, 2008. URL http://neuro-oncology.dukejournals.org; DOI: 10.1215/15228517-2008-001)*

Keywords: angiogenesis, glioblastoma multiforme, invasion, matrix metalloproteinase-2, survival

The matrix metalloproteinases (MMPs) are a large family of zinc-dependent endopeptidases that are involved in various aspects of tumor progression. Historically, they were believed to function as enzymes that degrade structural components of the extracellular matrix (ECM). Congruently, MMPs in cancer were first associated with tumor cell invasion and metastasis by enabling tumor cells to invade through the ECM and vascular basement membrane. It is now well established that MMPs exert diverse biological properties that are far beyond mere ECM degradation. MMPs cleave a variety of different substrates, including other MMPs, cytokines, growth factors, and receptors, as well as other non-ECM proteins.[1] Thereby, they can control tumor cell proliferation and survival and regulate new blood vessel growth in tumors.[2] Prominent MMP members are

Received April 30, 2007; accepted October 24, 2007.

Address correspondence to Gabriele Bergers, University of California San Francisco, Department of Neurological Surgery, 513 Parnassus Ave., Box 0520, San Francisco, CA 94143-0520, USA (gabriele.bergers@ucsf.edu).

the gelatinases, MMP-2 and MMP-9, which have been associated predominantly with the ability of tumors to invade and become neovascularized.[3] Consistent with those findings, increased MMP-2 and MMP-9 activity is often found in more aggressive tumors[4,5] and is associated with poor prognosis[6] in a variety of cancers, including human gliomas.[7] While there is increasing evidence about the pleiotropic effects of MMP-9, much less is known about the diverse functions of MMP-2.[8,9] Recently, MMP-2 was identified as one of four genetic markers that are expressed in glioblastoma multiforme (GBM) but not anaplastic astrocytoma.[10] Congruent with this observation, other studies found MMP-2 activity to increase with the grade of the glioma.[11] In addition to correlation studies in human cancers, in vitro studies have demonstrated the role of MMP-2 in tumor invasion and angiogenesis, in which induction of MMP-2 enhances invasiveness of ovarian cancer cells and exogenous MMP-2 increases tube formation by endothelial cells.[12] Further evidence of the involvement of MMP-2 in tumor angiogenesis was found in transgenic studies in which the growth of subcutaneous melanoma and lung carcinoma cell lines implanted into MMP-2 knockout (MMP-2ko) mice was delayed and tumor vessel density was reduced compared with tumor growth in MMP-2–proficient animals.[13] These studies, however, did not generate a completely MMP-2–deficient scenario since the implanted tumor cells were still able to express MMP-2. In summary, these correlative studies support the notion that MMP-2 in tumors is involved in angiogenesis, but its exact function in blood vessel formation remains largely unknown.

We previously generated genetically engineered wild-type (WT)-GBMs by isolating astrocytes from the hippocampus of neonatal mice and transforming them with the oncogenes *SV40 large T-antigen* and *V12–H-ras*.[14] When WT-GBM cells were injected intracranially into the striatum of mice, they developed into aggressive GBMs that exhibited all the major hallmarks of human GBMs. WT-GBM cells grew as invasive, highly angiogenic tumors with a leaky, tortuous vasculature and with hypoxic and pallisading necrotic centers within the tumor mass.[14] Notably, WT-GBM, like human GBM, infiltrated as single cells into the brain parenchyma and moved along basement membranes, preferentially along blood vessels. We found that MMP-2 was expressed in endothelial cells and tumor cells, reflecting its expression pattern in human GBMs. Because MMP-2ko mice are viable and fertile, we were able to generate MMP-2ko GBM cells using the same technique as described above in order to study the impact of MMP-2 loss in tumor cells and/or host cells by comparing propagation of WT-GBM and MMP-2ko GBM in both MMP-2–proficient and MMP-2ko hosts. Our studies reveal that MMP-2 regulates vascular patterning and branching, thereby affecting tumor cell survival and tumor invasion in a dose-dependent manner in GBM.

Materials and Methods

Generation of MMP-2ko–Transformed Mouse Astrocytes

Primary astrocytes were isolated from 1- to 2-day-old WT and MMP-2ko/ko FvBN Ragko mice as described previously.[14]

Soft Agar Assay

Cells were plated in triplicate in a six-well plate at 5,000 cells/well, mixed in 0.35% low-melting-temperature agarose (Cambrex Bioscience, Rockland, ME, USA). After culturing cells for 14 days, the wells were stained with 0.005% crystal violet for 2 h and analyzed for colony number and size.

Intracranial Implantation of Astrocytes

Thirty-two Ragko and MMP-2ko Ragko mice, 6–8 weeks of age, were implanted intracranially with 2.5 µl of 0.7×10^6 WT or MMP-2ko/ko-transformed astrocytes as previously described.[14] Mice were anesthetized and heart-perfused with 4% paraformaldehyde (PFA) and/or phosphate-buffered saline (PBS). All implantation experiments were repeated up to three times for a total of 6–12 mice per group.

Tissue Preparation

For fixed sections, animals were heart-perfused with 4% PFA. The brains were fixed in formalin overnight and then immersed in 70% ethanol and embedded into paraffin, or immersed in 30% sucrose/PBS overnight, embedded in OCT freezing medium, and stored at –80°C. For unfixed sections, brains were embedded in OCT medium after heart perfusion with PBS.

Substrate Zymography

Tumors were removed from the brain, weighed, and then homogenized (1:3 wt/vol) in RIPA lysis buffer containing 20 mM Tris-HCl, pH 8.0, 137 mM NaCl, 10% glycerol, 1% Triton X-100, 0.1% sodium dodecyl sulfate (SDS), and 1× Roche complete protease inhibitor cocktail (Roche Applied Science, Indianapolis, IN, USA). Equivalent amounts of soluble extracts were analyzed by gelatin zymography on 10% SDS-polyacrylamide gels copolymerized with 1 mg/ml gelatin in sample buffer (5% SDS, 0.25 M Tris-HCl, 25% glycerol, 0.1% bromophenol blue, pH 6.8). After electrophoresis, gels were washed for 40 min in 2.5% Triton X-100, rinsed in water, and incubated for 16 h at 37°C in gelatinase buffer (50 mM Tris-HCl, pH 7.5, 5 mM $CaCl_2$, 1 µM $ZnCl_2$). Gels were then stained in Coomassie Brilliant Blue R-250 staining solution (Bio-Rad, Hercules, CA, USA) and destained in a solution of 30% ethanol and 10% acetic acid. Negative staining denotes the locations of active proteinase bands. Ethylenediaminetetraacetic

acid (EDTA; 20 mM), which chelates magnesium and thereby inactivates MMPs, was added to the gelatinase buffer overnight to confirm that the proteases were metalloproteinases.

Histopathological Analysis

Hematoxylin and eosin staining was done in three whole-brain tumor samples for each tumor/host combination and analyzed by a neuropathologist who was blinded to the tumor/host types. Tumors were graded for mitoses, nuclear pleomorphism, necrosis, microperivascular spread, subarachnoid spread, white matter spread, and single cell/perineuronal spread.

Proliferation rate was determined by calculating the ratio of Ki-67–positive cells to all tumor cells per high-power field (×40) in three to eight tumor samples, and three to five high-power fields per sample for each tumor/host combination. Apoptotic indices were obtained by calculating the ratio of cells identified as positive by terminal deoxynucleotidyl transferase-mediated dUTP nick-end labeling (TUNEL) to all tumor cells per high-power field (×40) in three to seven tumor samples, and three to six high-power fields per sample for each tumor/host combination.

Invasiveness of tumors was determined by staining tumor cells with an antibody for SV40 large T-antigen on whole-brain sections. Tumors were graded from 1 to 3, where 1 indicates minimal distant spread of tumor cells and 3 indicates substantial and marked distant spread. Five to eight tumor samples per tumor/host combination were analyzed.

Infiltration was quantified by counting the number of infiltrating cells at the invasive edge (×20 field) in 50-μm frozen sections that were double-stained with large T-antigen and CD31. Infiltrating cells were defined as single cells at the invasive edge that were not associated with a blood vessel. Two to four different tumor samples and 3–10 sections per sample were analyzed per group.

Visualization of the vasculature was revealed by injecting mice intravenously with 0.05 mg fluorescein- or rhodamine-conjugated *Lycopersicon esculentum* (tomato) lectin (Vector Laboratories, Burlingame, CA, USA) and subsequent heart perfusion with 4% PFA and/or PBS. Brains were frozen in OCT and sectioned at 15 μm and 50 μm thicknesses. Vessel density was determined by calculating the area of CD31 staining using an ImageJ v1.34 software program (NIH) in ×20 fields of two to five different tumor samples per group and three to seven different sections per tumor sample.

Quantification of pericyte coverage was performed by collecting fluorescent images of tumor sections on a Zeiss Axioskop 2 with ×20 Plan Neofluar lenses and a Zeiss Axiocam color charge-coupled device. Red, green, and blue staining was quantitatively evaluated using ImageJ v1.34 software. The total area of CD31, desmin, or α-smooth muscle actin (α-SMA) staining was obtained. The fraction of pericyte coverage was calculated as the ratio of the area of desmin or α-SMA staining (red) to the area of CD31 staining (green). For desmin staining, 8–17 tumor sections per group were evaluated. For α-SMA staining, four to nine tumor sections per group were evaluated.

Immunohistochemical Analyses

Frozen (15 μm and 50 μm thickness) and paraffin (6 μm thickness) sections were used for immunohistochemical analysis. Fixed frozen sections were postfixed with 4% PFA, unfixed frozen sections were fixed with 100% methanol at –20°C, and paraffin sections were deparaffinized and subjected to graded rehydration. Astrocytoma cells were identified with a rabbit anti-SV40 T-antigen antibody (1:500; a gift from Dr. Douglas Hanahan, University of California San Francisco). Endothelial cells were visualized with a rat antimouse CD31 antibody (1:100; BD Biosciences Pharmingen, San Jose, CA, USA) in frozen sections and an antimouse endoglin antibody (R&D Systems, Minneapolis, MN, USA) in paraffin sections. Vascular endothelial growth factor receptor 2 (VEGFR2) staining was carried out on paraffin-embedded sections with a goat antimouse VEGFR2 antibody (1:50, R&D Systems). VEGF-VEGFR2 complex was visualized in frozen sections with mouse monoclonal antibody Gv39M (1:50; EastCoast Bio, North Berwick, ME, USA). Apoptotic cells were assessed on both paraffin and frozen sections by TUNEL staining as previously described.[15] Proliferating cells were detected on both paraffin and frozen sections with a rat antimouse Ki-67 antibody (1:100; DAKO Corp., Carpinteria, CA, USA). Pericytes were identified with a mouse antihuman desmin (1:100; DAKO Corp.) and mouse antihuman SMA (1:500; DAKO Corp.). Primary antibody reaction products were visualized with respective biotinylated secondary antibodies (1:200; Vector) and then incubated with an ABC kit and 3,3-diaminobenzidine chromophore (Vector). For fluorescent visualization of antibody reactions, secondary antibodies were labeled with fluorochrome AlexaFluor350, AlexaFluor488, or AlexaFluor594 (1:200; Molecular Probes, Eugene, OR, USA). Photomicrographs were taken with a Zeiss Axiovert 2 microscope, using Openlab 3 software (Improvision, Lexington, MA, USA). Levels in images were adjusted in Adobe Photoshop 7.

Fluorescence-Activated Cell Sorting Analysis

After the mice were euthanized, tumors were removed from the brain. Tumors were minced with a razor blade and digested at 37°C for 30 min with 20 ml enzyme mixture containing minimal essential medium with Earle's balanced salt solution, 1 mM L-cysteine, 0.5 mM EDTA, 1 μg/ml DNAse I (Worthington Biochemical Corp., Lakewood, NJ, USA), and 20 U/ml papain (Worthington). Cells from the digested tumors were passed through a 70-μm cell strainer and washed with Dulbecco's modified Eagle's medium. Red blood cells were lysed with PharmLyse (BD Biosciences Pharmingen) and washed. Cell pellets were resuspended in PBS containing 1% bovine serum albumin. Cells were incubated with primary antibodies on ice. The following primary antibodies were used (all from BD Biosciences Pharmingen): phycoerythrin-CD31 (1:50), rat antimouse CD11b

(1:50), rat antimouse Ly-6G (GR1 antigen) (1:60), and rabbit antimouse CD45 (1:50). If the primary antibody was unlabeled, secondary antibodies fluorescently labeled with the fluorochrome AlexaFluor647 (1:100; Molecular Probes) were added to the cell suspension.

RNA Isolation, Reverse Transcriptase PCR, and Real-Time PCR Analysis

RNA isolation was performed on cells sorted via fluorescence-activated cell sorting (FACS), on cell cultures, and on whole tissue. FACS-sorted cells and cells obtained from culture were placed in a cell lysis solution containing β-mercaptoethanol (Qiagen Inc., Valencia, CA, USA). RNA was isolated following RNeasy Mini Kit protocols (Qiagen Inc.). Whole tissues were flash frozen in liquid nitrogen and stored at –80°C until required. After thawing tissue on ice, 1 ml of TRIzol reagent (Invitrogen, Carlsbad, CA, USA) was added, and the tissue was homogenized immediately using a rotor-stator homogenizer (Fisher-Scientific, Pittsburgh, PA, USA). Total RNA was harvested per the manufacturer's instructions. cDNA was used for qualitative PCR (Roche Diagnostic Corp., Indianapolis, IN, USA). The following primer sequences were used: For MMP-2, (F) 5'-CAGTGACACCACGTGACAAGC-3'; (R) 5'-GGCAGCATCTAGTTGCTGGAC-3'; 60°C. For the ribosomal protein L19, (F) 5'-CTGAAGGTCAAAGGGAATGTG-3'; (R) 5'-GGACAGAGTCTTGATGATCTC-3'; 58°C.

Quantitative real-time PCR analysis of VEGFR2 expression was performed using the iQ SYBR Green Supermix and iCycler thermocycler (Bio-Rad Laboratories), according to the manufacturer's instructions. To control for variations in input cDNA between samples, L19 amplifications were performed in parallel for normalization. All measurements were collected in triplicate and confirmed by independent experiments. Primers for real-time PCR were, for VEGFR2, (F) 5'-GCGGGCTCCTGACTACAC-3'; (R) 5'-CCAAATGCTCCACCAACTCTG-3'; 60°C.

VEGF and VEGFR2 Western Blot Analysis

For VEGF Western blot analysis, proteins from 45-μg WT-GBM and MMP-2ko GBM tumor extracts, 15-μg WT-GBM and MMP-2ko GBM astrocyte supernatants, and 20-μg WT-GBM and MMP-2ko GBM astrocyte cell extracts were separated by SDS-polyacrylamide gel electrophoresis in 15% Tris-tricine gels and transferred to Immobilon-P membranes (Millipore Corp., Bedford, MA, USA) using 20% methanol. Blots were incubated with epitope-specific rabbit anti-VEGF antibody (provided by Donald Senger, Beth Israel Deaconess Medical Center).[16] VEGF protein was detected as previously described.[17] Anti-α-tubulin antibody was used to control for equal protein loading (1:5,000; Calbiochem Brand, EMD Biosciences, San Diego, CA, USA) in tumor and cell extracts. Equal amounts of proteins were loaded for astrocyte supernatants. For VEGFR2 Western blot analysis, 100 μg protein from WT-GBM and MMP-2ko GBM tumor extracts were loaded and separated on 15% Tris-glycine gels. Proteins were transferred to Immobilon-P using 5% methanol to ensure transfer of proteins with higher molecular weight. VEGFR2 was detected using an anti-VEGFR2 antibody (1:1,000; Cell Signaling Technology, Danvers, MA, USA).

Nonradioactive In Situ Hybridization

Nonradioactive in situ hybridization of RGS-5 was performed as previously described.[17]

Supplemental Material and Methods

For the soft agar assay, cells were plated in triplicate in a six-well plate at 5×10^5 cells/well, mixed in 0.35% low-melting-point agarose (Invitrogen). After culturing the cells for 21 days, the wells were stained with 0.005% crystal violet for 4 h and analyzed for colony number and size. Insulin-like growth factor binding protein-2 (IGFBP-2) Western blots were performed as described for VEGF Western blot analysis using an anti-IGFBP-2 antibody (1:500; AF 797, R&D Systems) and an anti-α-tubulin antibody.

Statistical Analysis

All experiments were repeated two to four times. Statistical analyses were performed over all groups with the Kruskal-Wallis *H*-test to determine statistical significance using $p < 0.05$ followed by a Mann-Whitney *U*-test for pairwise comparison. A *p* value (exact significance) of <0.05 was considered statistically significant. Kaplan-Meier curves and the log-rank test were used to compare survival times among various groups of mice. All calculations were performed using SPSS version 11.0 (SPSS Inc., Chicago, IL, USA).

Results

MMP-2 Activity in GBMs Originates from Tumor and Host Cells

We first demonstrated the presence of MMP-2 activity in WT-GBM tumors by gelatin zymography (Fig. 1A, a) and determined its RNA expression pattern by separating tumor cells, endothelial cells ($CD31^+/CD11b^-$), and monocytic cells ($CD45^+$) from WT-GBM tumors by FACS (Fig. 1A, b). Gelatin zymography revealed that modest MMP-2 levels existed in the tumors as the larger pro-MMP-2 form and as the activated shorter form (Fig. 1A, a). Using reverse transcriptase (RT)-PCR analysis, we detected MMP-2 not only in tumor and endothelial cells, but also in $CD45^+$ myeloid cells. These data indicated that the MMP-2 expression pattern in our model of genetically engineered mouse GBM was similar to that observed in human gliomas.[11,18] They also suggested that MMP-2 could potentially have pleiotropic effects in GBM biology, specifically in the onset or maintenance of angiogenesis and in tumor cell invasion, based on its expression in endothelial, myeloid, and tumor cells.

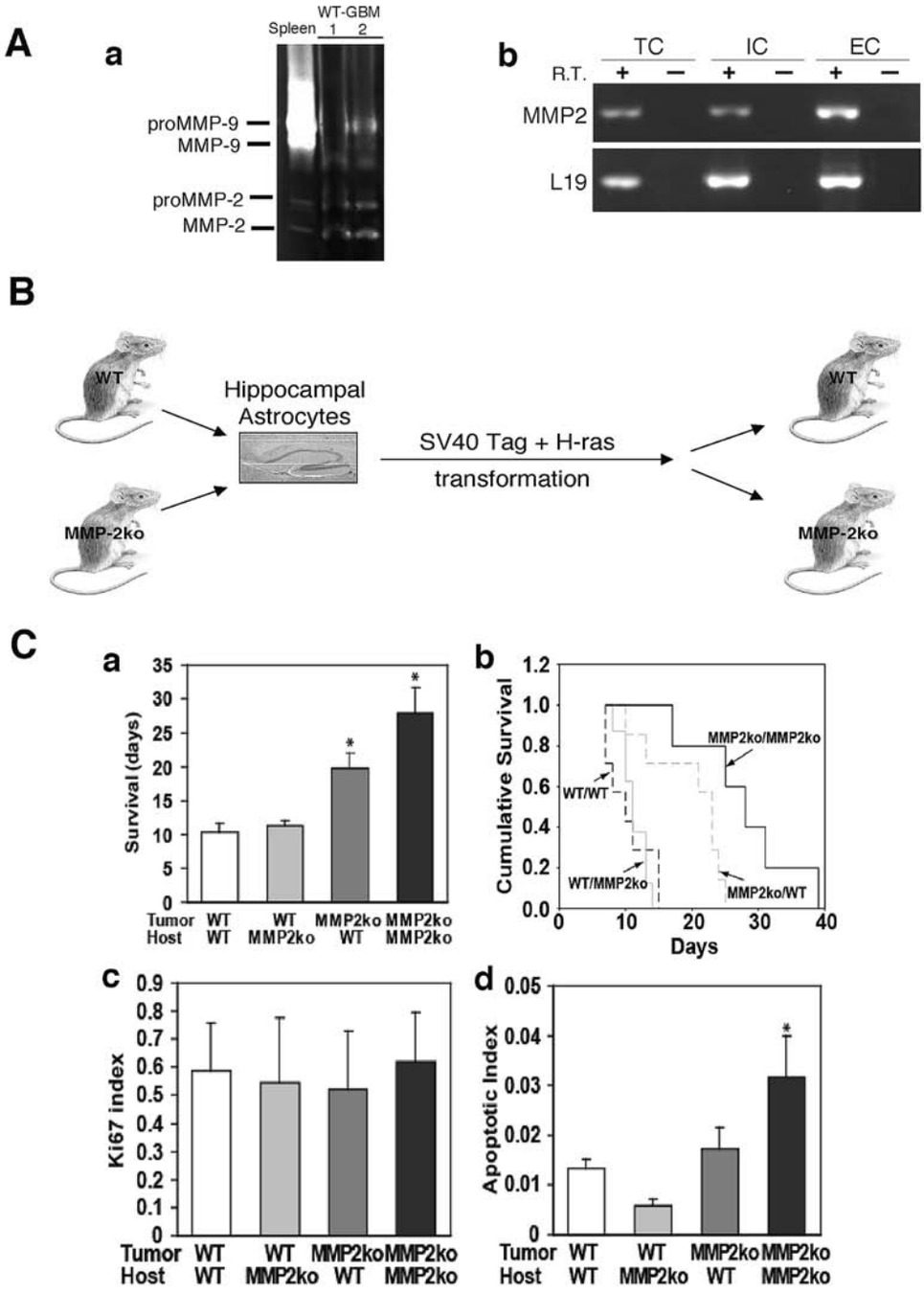

Fig. 1. Generation of matrix metalloproteinase MMP-2 deficiency in tumor and/or host cells and effects on tumor propagation. (A) (a) Gelatin zymography profiles of MMP-2 and MMP-9 activity in two independent wild-type glioblastoma multiforme (WT-GBM) orthotopic tumors. Protein extracts from mouse spleen were loaded alongside as controls for latent and active MMP-2 (72 and 62 kDa, respectively) and MMP-9. (b) Fluorescence-activated cell sorting was used to separate tumor cells (TC), $CD31^+$, $Gr1^-$ endothelial cells (EC), and $CD45^+$ monocytic inflammatory cells (IC). The isolated cell populations were tested for MMP-2 transcription by reverse transcriptase (RT)-PCR. The ribosomal protein L19 was used as an internal control, and reactions were performed without RT as negative controls. (B) Schematic representation of MMP-2 knockout (MMP-2ko) GBM and WT-GBM cell line generation. Four distinct groups were analyzed and compared to each other: WT-GBM in WT mice; WT-GBM in MMP-2ko mice, MMP-2ko GBM in WT mice, and MMP-2ko GBM in MMP-2ko mice. (C) MMP-2 deficiency increases survival of GBM-bearing mice in a dose-dependent manner. (a) WT and MMP-2ko mice bearing an MMP-2ko GBM had significantly increased survival over mice with WT tumors, by 1.9-fold ($p = 0.007$) and 2.7-fold ($p = 0.001$), respectively. (b) Kaplan-Meier survival curves for WT mice with WT-GBM, and MMP-2ko mice with MMP-2ko GBM showed a significant difference in survival ($p = 0.001$). (c) Ki-67 or proliferative indices for four tumor/host combinations showed no difference among the four groups. (d) Apoptotic indices for the four groups exhibited a 2.4-fold increase in apoptosis when MMP-2 activity was completely abolished in the host and tumor cell compartment ($p = 0.056$). Error bars represent SEM.

Generation of MMP-2ko GBMs

Since MMP-2 is expressed in both normal host and tumor cells, we intended to generate a system in which MMP-2 is deleted in all cell types. We generated a GBM cell line that lacks MMP-2 activity by isolating astrocytes from MMP-2ko neonatal mice and transforming the astrocytes with the oncogenes *SV40 large T-antigen* and *V12–H-ras* (Fig. 1B). For controls, we employed WT-GBM cells that were generated in the same way, but with astrocytes isolated from WT, MMP-2–proficient mice.[14] We confirmed that both WT-GBM and MMP-2ko GBM cell lines had a similar transformation status by performing soft agar assays, which showed that both cell lines gave rise to similar numbers of soft agar colonies (see supplementary data, Fig. S1). Furthermore, both cell lines exhibited comparable levels of *SV40 large T-antigen* and *H-ras* oncogene expression (see supplementary data, Fig. S1).

GBM-Bearing Mice Have a Survival Benefit in the Complete Absence of MMP-2

We next assessed whether MMP-2 affects survival of GBM-bearing mice. We first injected MMP-2ko GBM cells into an MMP-2ko host (MMP-2ko^{T}/MMP-2ko^{H}). In the complete absence of MMP-2, GBM-bearing mice had a three- to fourfold increase in survival benefit when compared to the WT situation ($p = 0.001$) in which WT-GBM cells were injected into MMP-2–proficient WT mice (WT^{T}/WT^{H}) (Fig. 1C, a and b). We then generated heterozygous scenarios (Fig. 1B) in which we either injected WT-GBM cells into an MMP-2ko host (WT^{T}/MMP-2ko^{H}), or MMP-2ko GBM cells into an MMP-2–proficient WT host (MMP-2ko^{T}/WT^{H}). While the survival rate of the WT^{T}/MMP-2ko^{H} group was comparable to that of the WT^{T}/WT^{H} group, the mean survival of the MMP-2ko^{T}/WT^{H} group was twice as long as the mean survival of the WT^{T}/WT^{H} group ($p = 0.007$, Fig. 1C, a,b). Thus, removing MMP-2 from the tumor cells alone had a significant effect on survival. As illustrated in Fig. 1C (b), Kaplan-Meier survival curves confirmed that the MMP-2ko^{T}/MMP-2ko^{H} and MMP-2ko^{T}/WT^{H} groups had higher survival rates than the WT^{T}/WT^{H} group ($p = 0.001$).

Neuropathological analysis showed that all tumors in each of the four groups exhibited typical features of high-grade astrocytomas, including high numbers of mitotic figures and cellular pleomorphism/atypia. Surprisingly, pallisading necrosis was observed in tumors of the WT and heterozygous groups but not in tumors that were completely deficient in MMP-2 (MMP-2ko^{T}/MMP-2ko^{H} group) (data not shown). The absence of necrosis may be partly related to the absence of infiltration by tumor cells into the brain parenchyma.[19] We then assessed the proliferative rate of the tumors from each of the four groups, but did not find any statistically significant differences between the growth rate of tumors that lost MMP-2 activity (either in the tumor or in host cells) and the growth rate of those that maintained MMP-2 activity (Fig. 1C, c). We did detect, however, a 2.4-fold increase in the apoptotic rate of GBMs that were completely deficient in MMP-2 ($p = 0.056$), which most likely contributed to the slower growth of the tumors in the MMP-2ko^{T}/MMP-2ko^{H} group (Fig. 1C, d). The elevated numbers of apoptotic cells were observed only in the complete absence of MMP-2, implying that MMP-2 deficiency in either tumor cells or host cells alone was not sufficient to increase apoptosis in GBM. The increased apoptotic ratio in tumors when MMP-2 activity is completely abolished might suggest that MMP-2 is linked to a tumor survival factor. Indeed, MMP-2 and other metalloproteinases have been shown to degrade IGFBP-2, unmasking insulin-like growth factors that act as cell survival factors.[20,21] We investigated IGFBP-2 levels in the presence and absence of MMP-2 by Western blot analyses and found that IGFBP-2 in tumors is degraded to a similar extent independent of MMP-2 (see supplementary data, Fig. S2).

MMP-2 Affects Vascular Density by Regulating Blood Vessel Branching

MMP-2 can potentially mediate tumor cell survival by regulating the activity of survival factors or by supporting new blood vessel formation during tumor propagation. To elicit whether MMP-2 affects GBM neovascularization, we sought to visualize and compare the vascular network in GBMs in the presence and absence of MMP-2 (Fig. 2A–D). We found that the vasculature in WT-GBM tumors, independent of the MMP-2 status of the host, had undergone vascular remodeling as in human GBMs. Tumor vessels of GBMs in the WT^{T}/MMP-2ko^{H} group (Fig. 2B) were hyperdilated and irregularly shaped, as were tumor vessels of the WT^{T}/WT^{H} group (Fig. 2A). A subtle difference could be observed in tumor vessels of GBM from the MMP-2ko^{T}/WT^{H} cohort that looked somewhat irregular and leaky, but also exhibited a mild increase in vessel density ($p = 0.023$), as well as some normalization of vessel morphology to slightly thinner and less tortuous vessels (Fig. 2C). The complete absence of MMP-2 in both tumor and host cells, however, led to a dramatic and unexpected change in both vessel morphology and density. GBM blood vessels from the MMP-2ko^{T}/MMP-2ko^{H} cohort were three- to fourfold denser than vessels from all other groups ($p = 0.001$) and formed a highly branched and slim vascular network (Fig. 2D). Thus, there appears to be an MMP-2 dose response, but the complete absence of MMP-2 is required to completely alter the vascular phenotype. It was puzzling that tumor cells in such a vascular-rich environment were more prone to apoptosis, raising the question of whether these blood vessels are functionally impaired.

MMP-2 Affects VEGFR-2 Levels in Tumors

When blood vessels undergo vascular remodeling, they become activated and form new sprouts. In this process, endothelial cells and pericytes, the perivascular support cells, become activated. The activation of the endothelial cells can be determined by the presence of the VEGF-VEGFR2 complex formation on the endothelial

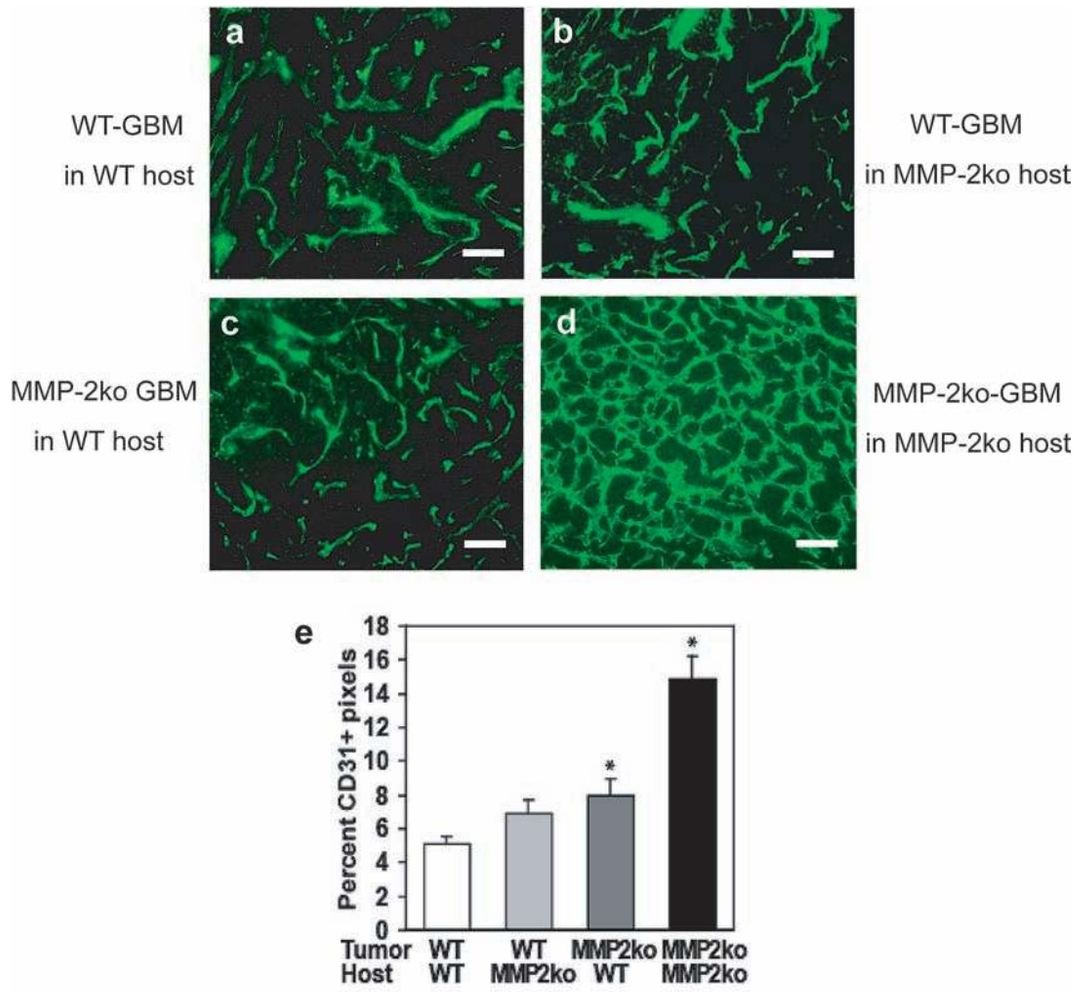

Fig. 2. The matrix metalloproteinase MMP-2 in glioblastoma multiforme (GBM) regulates tumor angiogenesis by affecting vascular branching. Blood vessels are visualized by fluorescein isothiocyanate–lectin perfusion and CD31 staining (green) of wild-type (WT)-GBM in WT host (A), WT-GBM in MMP-2 knockout (MMP-2ko) host (B), MMP-2ko GBM in WT host (C), and MMP-2ko GBM in MMP-2ko host (D). (E) Quantitative analysis of blood vessel density in GBM revealed a significant increase of blood vessels in both the MMP-2ko GBM in WT host group ($p = 0.023$) and the MMP-2ko GBM in MMP-2ko host group ($p < 0.001$). Error bars represent SD.

cells.[22,23] Using an antibody that specifically recognizes the VEGF-VEGFR2 complex as opposed to the ligand or receptor itself,[22] we found that tumor vessels from both WT^T/WT^H and $MMP\text{-}2ko^T/MMP\text{-}2ko^H$ cohorts showed VEGF-VEGFR2 complex formation on endothelial cells (Fig. 3A). Both tumor types also expressed similar levels of $VEGF_{164}$, the predominant VEGF isoform in these tumors, but $MMP\text{-}2ko^T/MMP\text{-}2ko^H$ GBMs exhibited an approximately fourfold reduction in VEGFR2 levels as quantified by Western blot and quantitative RT-PCR analyses (Fig. 3B–D).

MMP-2 Regulates Pericyte Activation and Recruitment

In addition to the lower levels of VEGFR2 in tumors totally devoid of MMP-2, we found that pericytes did not become activated in GBMs of the $MMP\text{-}2ko^T/MMP\text{-}2ko^H$ group as assessed by the lack of RGS-5 expression (Fig. 3A). RGS-5 is a member of the RGS family of GTPase-activating proteins for G-proteins and is induced in developing and angiogenic pericytes in the brain and pancreas.[17,24,25] Furthermore, MMP-2ko GBM had approximately 30% to 40% less pericyte coverage of blood vessels than did WT-GBM (desmin, $p = 0.031$; α-SMA, $p = 0.001$), further supporting the notion that pericytes were not activated and recruited to the vascular site (Fig. 4A–F). Interestingly, although WT-GBM tumors contained more pericytes, their blood vessels were more dilated than those of MMP-2ko tumors, which contained fewer pericytes.

MMP-2 Affects Vascular Functionality in Tumors

The data suggested that in the absence of MMP-2, tumor vessels have lower levels of VEGFR2 but still undergo extensive vascular branching without recruitment and activation of pericytes, suggestive of impaired vascular maturation. Based on these findings, we speculated

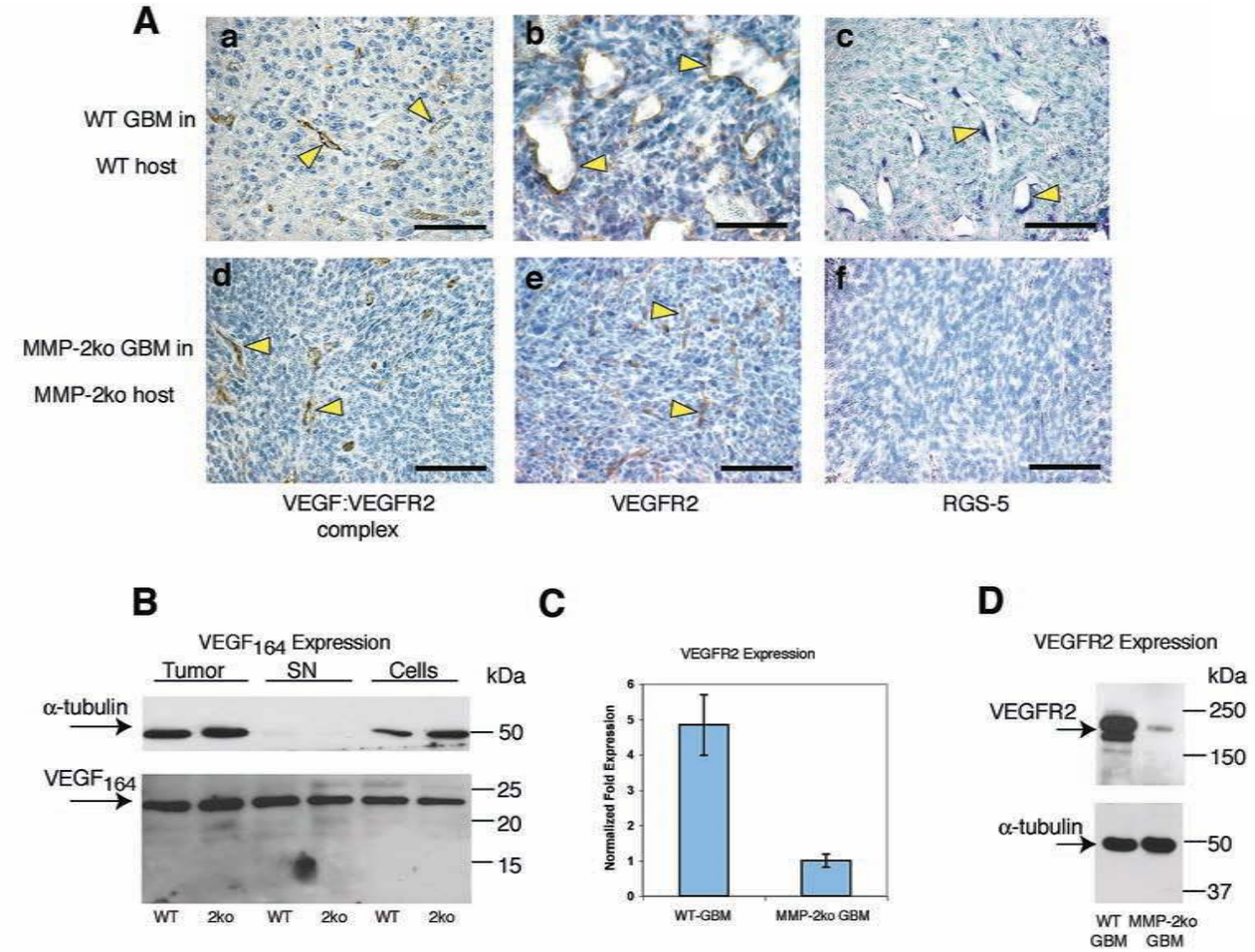

Fig. 3. Matrix metalloproteinase MMP-2–deficient tumors undergo vascular remodeling but are dysfunctional and fail to activate pericytes. (A) Activated tumor blood vessels were detected by the presence of the vascular endothelial growth factor (VEGF)–vascular endothelial growth factor receptor 2 (VEGFR2) complex (brown) in wild-type glioblastoma multiforme (WT-GBM) in WT host (a) and MMP-2 knockout glioblastoma multiforme (MMP-2ko GBM) in MMP-2ko host (d). Both tumor/host groups expressed VEGFR2 (b,e). Activated, angiogenic pericytes on blood vessels were detected by RGS-5 transcription on tumor sections. RGS-5$^+$ tumor pericytes were abundant in WT-GBMs (c) but were not present when MMP-2 activity was completely abolished in GBM (f). Scale bars = 83 μm. (B) Western blot analysis revealed that WT-GBM tumors and cell lines, as well as MMP-2ko tumors and cell lines, both produced equivalent levels of $VEGF_{164}$. Equivalent protein concentrations were loaded and α-tubulin was used as an additional protein loading control for tumor and cell lysates. (C) VEGFR2 RNA expression levels were reduced 4.8-fold in MMP-2ko GBMs compared to WT-GBMs, as determined by quantitative reverse transcriptase PCR. (D) Western blot analysis of tumor extracts revealed a reduction of VEGFR2 protein levels in MMP-2ko GBMs compared to WT-GBMs; α-tubulin was used as a protein loading control in tumor lysates.

that the angiogenic tumor vasculature in tumors devoid of MMP-2 might not be very functional. We therefore assessed vessel functionality by visualizing the ability of tumor vessels to perfuse fluorescein isothiocyanate (FITC)-lectin and compared it to the complete numbers of tumor vessels as indicated by anti-CD31 staining (Fig. 4G). While WT-GBM displayed a predominant overlap of FITC-lectin and CD31 staining in tumor vessels (normal vessels are shown as controls), MMP-2ko GBMs were much less perfused, although they showed a high degree of CD31$^+$ tumor vessels. In contrast, normal brain vessels adjacent to MMP-2ko tumors were well perfused.

MMP-2 Affects Tumor Cell Infiltration and Perivascular Tumor Cell Invasion

Finally, we observed that MMP-2 affected the invasive behavior of GBMs. GBMs are highly invasive tumors that can infiltrate as single cells into the brain parenchyma and can invade along basement membranes, including the leptomeninges, ventricles, and vascular basement membranes. WT-GBM exhibited all of these invasive features (Fig. 5A), but in the complete absence of MMP-2, tumors surprisingly grew even more diffusely (Fig. 5B). We quantified the invasive pattern by grading and counting invading tumor cells, and by distinguishing between infiltrative tumor behavior, in which

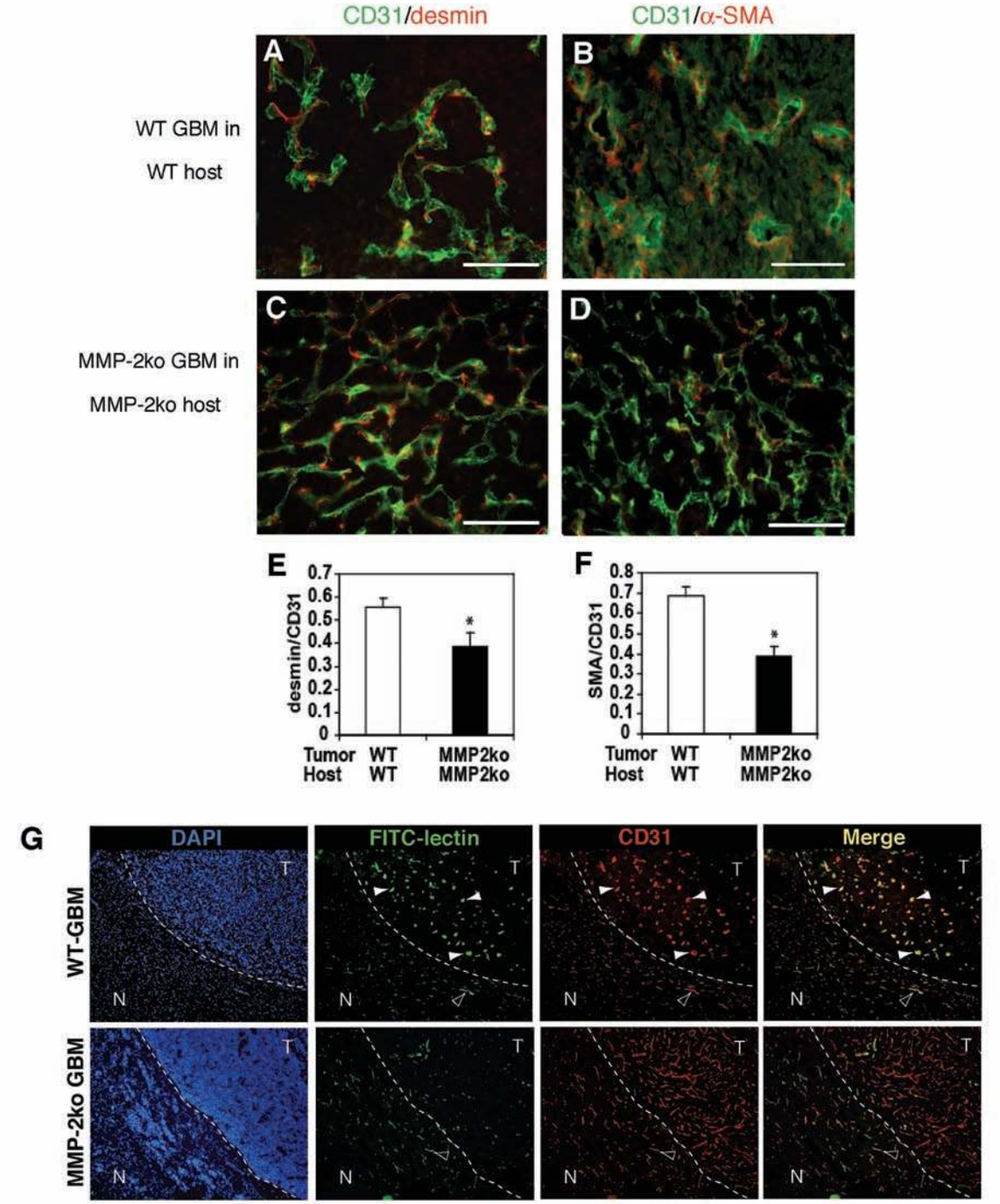

Fig. 4. Matrix metalloproteinase MMP-2 deficiency reduces pericyte coverage on glioblastoma multiforme (GBM) tumor vessels. Pericytes (red) were detected with desmin (A, C) and α-smooth muscle actin (α-SMA) antibodies (B, D). Blood vessels (green) were perfused with fluorescein isothiocyanate (FITC)-lectin and stained with FITC-CD31 antibody. Scale bars = 83 μm. (E, F) Quantification of the endothelial cell:pericyte ratio in GBM revealed a decrease in pericytes in the absence of MMP-2 (desmin, $p = 0.031$; α-SMA, $p = 0.001$). Error bars represent SEM. (G) Perfusion of tissues with FITC-lectin (green) before animal euthanization, followed by subsequent immunohistochemical staining for CD31 (red), suggests that the tumor vasculature in MMP-2 knockout (MMP-2ko) tumors is less functional than in wild-type (WT)-GBM tumors as represented by the relative lack of FITC-lectin staining in MMP-2ko GBMs. Vessels that co-stain for both lectin and CD31 are shown in yellow when merged (solid white arrowheads). Note the presence of lectin/CD31$^+$ functional vessels in the surrounding normal brain of both WT-GBMs and MMP-2ko tumors (outlined arrowheads). The border between tumor (T) and normal brain (N) is depicted by the dotted line.

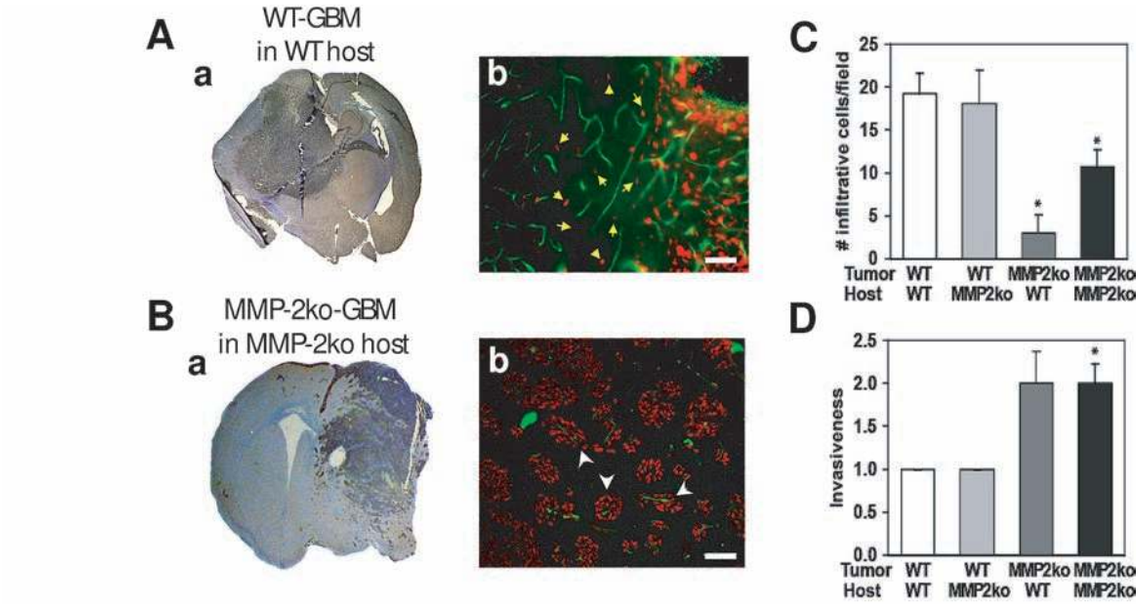

Fig. 5. Matrix metalloproteinase MMP-2 deficiency increases perivascular tumor invasion in glioblastoma multiforme (GBM). (A and B) (a, b) Tumor cells in the brain parenchyma were detected by SV40 T-antigen staining (brown or red), and vessels were visualized with fluorescein isothiocyanate (FITC)-lectin and an FITC-CD31 antibody (green). (B) In the absence of MMP-2, tumor cells became less infiltrative but became more invasive by moving along blood vessels. Scale bars = 83 μm. (C) Infiltration by tumor cells was measured by the number of single infiltrating cells at the tumor edge that were not associated with a blood vessel (yellow arrows in A,b). Infiltration was decreased in MMP-2 knockout (MMP-2ko) tumors in both wild-type (WT) ($p = 0.004$) and MMP-2ko host ($p = 0.015$). (D) Perivascular invasion, defined as tumor cells associated with blood vessels (white arrowheads in B,b), was quantified on a scale from 1 to 3 where 1 = minimal, 2 = moderate, and 3 = extensive perivascular invasion. MMP-2ko GBM were more perivascular invasive than WT-GBM in WT hosts ($p = 0.065$) or MMP-2ko hosts ($p = 0.030$). Error bars represent SEM.

tumor cells infiltrate into the brain parenchyma without being in contact with blood vessels (Fig. 5A, a, yellow arrows), and perivascular invasion, in which tumor cells move into the normal tissue by moving along and being closely associated with blood vessels (Fig. 5B, b, white arrowheads). We found that GBMs from the WT^T/WT^H and $WT^T/MMP\text{-}2ko^H$ groups were equally infiltrative, whereas tumors from the $MMP\text{-}2ko^T/WT^H$ and $MMP\text{-}2ko^T/MMP\text{-}2ko^H$ cohorts were both much less infiltrative ($p = 0.004$ and $p = 0.015$; Fig. 5C). On the other hand, MMP-2ko tumors increased their perivascular invasion mode compared with WT controls ($p = 0.065$ and $p = 0.030$; Fig. 5D). In summary, loss of MMP-2 did not inhibit invasion, but altered the mode of diffuse tumor growth by causing tumor cells to preferentially move along blood vessels.

Discussion

We generated an orthotopic mouse model of GBM that was completely devoid of MMP-2 activity by producing transformed MMP-2ko astrocytes and implanting them intracranially into MMP-2ko mice. MMP-2–dependent effects appeared to be dose dependent irrespective of its expression pattern in host or tumor cells. However, we found that the complete loss of MMP-2 activity, seen in the $MMP\text{-}2ko^T/MMP\text{-}2ko^H$ group, resulted in markedly increased vascularity that was associated with increased angiogenic branching of tumor vessels in GBMs. Paradoxically, tumor cells in such a vascular-rich environment were more prone to apoptosis, and therefore tumor-bearing mice exhibited longer mean survival times in the absence of MMP-2. These results suggest that the dense and highly branched network of tumor vessels was not productive enough to support tumor growth. Further rationale for this hypothesis comes from several observations: First, tumor vessels in an MMP-2–devoid scenario express substantially less VEGFR2. Second, pericytes, the perivascular support cells that enable maturation and stabilization of newly formed blood vessels, were not activated in the angiogenic process, and MMP-2ko tumors contained fewer pericytes than did WT tumors. Third, tumor vessels of MMP-2ko GBM were less perfused than those of WT-GBM. Further support for the dysfunctionality of tumor vessels in the absence of MMP-2 stems from our observation that MMP-2ko tumors grew more diffusely by migrating along blood vessels into the brain parenchyma, a phenotype we also had observed in VEGF-deficient and hypoxia-inducible factor–deficient GBMs that do not undergo proper neovascularization.[14] Interestingly, recent studies have revealed that delta-like ligand 4 (Dll4) inhibitors, which block notch signaling in endothelial cells, affected tumors in a similar way: Tumor vessels became hypervascularized and hyperbranched, but were poorly perfused and nonfunctional in the presence of the Dll4 inhibitor, leading to reduced tumor growth.[26,27] Thus, MMP-2, like Dll4, could act as a negative regulator of vascular patterning and angio-

genesis in GBM. It is also possible that MMP-2 in GBM produces antiangiogenic peptides such as angiostatin and tumstatin[28] or regulates the activity of other proteins that are implicated in promoting new blood vessel growth. In addition to MMP-2's role in regulating angiogenesis, MMP-2 could also have direct effects on tumor cell survival. The increased apoptotic ratio in tumors when MMP-2 activity is completely abolished might suggest that MMP-2 is linked to a tumor survival factor. Given that MMP-2 is involved in the degradation of IGFBP-2, thereby unmasking insulin-like growth factors that can act as cell survival factors,[20] we studied IGFBP-2 levels in the presence and absence of MMP-2 but were unable to observe substantial differences.

Finally, our observations that GBMs without MMP-2 activity grew slower and exhibited a significant increase in mean survival, although tumor cells still invaded predominantly along blood vessels, might make MMP-2 an attractive target for GBM therapy.

Acknowledgments

We thank Dr. Kathleen Lamborn for help with the biostatistical analyses, Dr. Donald Senger (Beth Israel Deaconess Medical Center) for the VEGF antibody, Bina Kaplan and James Hudock for mouse husbandry and tumor implantations, and Ilona Garner for help with the manuscript. This work was supported by grants from the NIH (RO1 CA113382, PO1 CA072006) and by startup funds to G.B. from the Department of Neurological Surgery at the University of California San Francisco.

References

1. Page-McCaw A, Ewald AJ, Werb Z. Matrix metalloproteinases and the regulation of tissue remodelling. *Nat Rev Mol Cell Biol*. 2007;8:221–233.
2. Mott JD, Werb Z. Regulation of matrix biology by matrix metalloproteinases. *Curr Opin Cell Biol*. 2004;16:558–564.
3. Djonov V, Cresto N, Aebersold DM, et al. Tumor cell specific expression of MMP-2 correlates with tumor vascularisation in breast cancer. *Int J Oncol*. 2002;21:25–30.
4. Talvensaari-Mattila A, Paakko P, Turpeenniemi-Hujanen T. Matrix metalloproteinase-2 (MMP-2) is associated with survival in breast carcinoma. *Br J Cancer*. 2003;89:1270–1275.
5. Brown PD, Bloxidge RE, Stuart NS, Gatter KC, Carmichael J. Association between expression of activated 72-kilodalton gelatinase and tumor spread in non-small-cell lung carcinoma. *J Natl Cancer Inst*. 1993;85:574–578.
6. Vaisanen A, Tuominen H, Kallioinen M, Turpeenniemi-Hujanen T. Matrix metalloproteinase-2 (72 kD type IV collagenase) expression occurs in the early stage of human melanocytic tumour progression and may have prognostic value. *J Pathol*. 1996;180:283–289.
7. Guo P, Imanishi Y, Cackowski FC, et al. Up-regulation of angiopoietin-2, matrix metalloprotease-2, membrane type 1 metalloprotease, and laminin 5 gamma 2 correlates with the invasiveness of human glioma. *Am J Pathol*. 2005;166:877–890.
8. Coussens LM, Fingleton B, Matrisian LM. Matrix metalloproteinase inhibitors and cancer: trials and tribulations. *Science*. 2002;295:2387–2392.
9. Egeblad M, Werb Z. New functions for the matrix metalloproteinases in cancer progression. *Nat Rev Cancer*. 2002;2:161–174.
10. Zhou YH, Hess KR, Liu L, Linskey ME, Yung WK. Modeling prognosis for patients with malignant astrocytic gliomas: quantifying the expression of multiple genetic markers and clinical variables. *Neuro-oncol*. 2005;7:485–494.
11. Wang M, Wang T, Liu S, Yoshida D, Teramoto A. The expression of matrix metalloproteinase-2 and -9 in human gliomas of different pathological grades. *Brain Tumor Pathol*. 2003;20:65–72.
12. Zhang A, Meng L, Wang Q, et al. Enhanced in vitro invasiveness of ovarian cancer cells through up-regulation of VEGF and induction of MMP-2. *Oncol Rep*. 2006;15:831–836.
13. Itoh T, Tanioka M, Yoshida H, et al. Reduced angiogenesis and tumor progression in gelatinase A-deficient mice. *Cancer Res*. 1998;58:1048–1051.
14. Blouw B, Song H, Tihan T, et al. The hypoxic response of tumors is dependent on their microenvironment. *Cancer Cell*. 2003;4:133–146.
15. Naik P, Karrim J, Hanahan D. The rise and fall of apoptosis during multistage tumorigenesis: down-modulation contributes to progression from angiogenic progenitors. *Genes Dev*. 1996;10:2105–2116.
16. Sioussat TM, Dvorak HF, Brock TA, Senger DR. Inhibition of vascular permeability factor (vascular endothelial growth factor) with antipeptide antibodies. *Arch Biochem Biophys*. 1993;301:15–20.
17. Berger M, Bergers G, Arnold B, Hammerling GJ, Ganss R. Regulator of G-protein signaling-5 induction in pericytes coincides with active vessel remodeling during neovascularization. *Blood*. 2005;105:1094–1101.
18. Thorns V, Walter GF, Thorns C. Expression of MMP-2, MMP-7, MMP-9, MMP-10 and MMP-11 in human astrocytic and oligodendroglial gliomas. *Anticancer Res*. 2003;23:3937–3944.
19. Brat DJ, Castellano-Sanchez AA, Hunter SB, et al. Pseudopalisades in glioblastoma are hypoxic, express extracellular matrix proteases, and are formed by an actively migrating cell population. *Cancer Res*. 2004;64:920–927.
20. Minuto F, Palermo C, Arvigo M, Barreca AM. The IGF system and bone. *J Endocrinol Invest*. 2005;28:8–10.
21. Nakamura M, Miyamoto S, Maeda H, et al. Matrix metalloproteinase-7 degrades all insulin-like growth factor binding proteins and facilitates insulin-like growth factor bioavailability. *Biochem Biophys Res Commun*. 2005;333:1011–1016.
22. Brekken RA, Huang X, King SW, Thorpe PE. Vascular endothelial growth factor as a marker of tumor endothelium. *Cancer Res*. 1998;58:1952–1959.
23. Ferrara N, Gerber HP, LeCouter J. The biology of VEGF and its receptors. *Nat Med*. 2003;9:669–676.
24. Bondjers C, Kalen M, Hellstrom M, et al. Transcription profiling of platelet-derived growth factor-B-deficient mouse embryos identifies RGS5 as a novel marker for pericytes and vascular smooth muscle cells. *Am J Pathol*. 2003;162:721–729.
25. Bergers G, Song S. The role of pericytes in blood-vessel formation and maintenance. *Neuro-Oncology*. 2005;7:452–464.
26. Noguera-Troise I, Daly C, Papadopoulos NJ, et al. Blockade of Dll4 inhibits tumour growth by promoting non-productive angiogenesis. *Nature*. 2006;444:1032–1037.
27. Ridgway J, Zhang G, Wu Y, et al. Inhibition of Dll4 signalling inhibits tumour growth by deregulating angiogenesis. *Nature*. 2006;444:1083–1087.
28. Kalluri R. Basement membranes: structure, assembly and role in tumour angiogenesis. *Nat Rev Cancer*. 2003;3:422–433.